Chapter 5 Phase simulation of the Fe-Cr alloy system

Capítulo 5 Simulación de las Fases del sistema de aleación Fe-Cr

SORIANO-VARGAS, Orlando †*, LOPEZ-HIRATA, Víctor M., CAYETANO-CASTRO, Nicolas and CASTREJON-SANCHEZ, Víctor H.

[1]Tecnológico de Estudios Superiores de Jocotitlán, Carretera Toluca Atlacomulco km 44.8, Ejído de San Juan y San Agustín, Jocotitlán, México.
[2]Instituto Politécnico Nacional (ESIQIE), Apdo. Postal 118-395, Mexico, D.F. 07300
[3]CNMN, Instituto Politécnico Nacional, Wilfrido Massieu s/n, UPALM, Gustavo A. Madero, Ciudad de México 07738, México.

ID 1st Author: *Orlando, Soriano-Vargas* / **ORC ID**: 0000-0002-9331-7909

ID 1st Co-author: *Víctor M., López-Hirata* / **ORC ID**: 0000-0002-7781-3419

ID 2nd Co-author: *Nicolas, Cayetano-Castro* / **ORC ID**: 0000-0003-4827-795X

ID 3rd Co-author: *Victor H., Castrejón-Sanchez* / **ORC ID**: 0000-0002-0112-5388

DOI: 10.35429/H.2022.3.65.83

*orlando.soriano@tesjo.edu.mx

A. Ledesma (AA.). Science of Technology and Innovation. Handbooks-TII-©ECORFAN-Mexico, 2022.

Abstract

Spinodal decomposition was studied during aging of Fe-Cr alloys by means of the numerical solution of the linear and nonlinear Cahn-Hilliard differential partial equations using the explicit finite difference method. Results of the numerical simulation permitted to describe appropriately the mechanism, microstructure, and kinetics of phase decomposition during the isothermal aging of these Fe-Cr alloys. The growth kinetics of phase transition was observed to occur very slowly during the early stages of aging, and it increased considerably as the aging progressed. The nonlinear equation was observed to be more suitable for describing the early stages of spinodal decomposition than the linear one.

Fe-Cr alloy, Spinodal insufficiency, Cahn-Hilliard equivalence, Thermal aging

Resumen

Se estudió la descomposición espinodal durante el envejecimiento de aleaciones de Fe-Cr mediante la solución numérica de las ecuaciones parciales diferenciales lineales y no lineales de Cahn-Hilliard utilizando el método explícito de diferencias finitas. Los resultados de la simulación numérica permitieron describir adecuadamente el mecanismo, morfología y cinética de descomposición de fase durante el envejecimiento isotérmico de estas aleaciones. Se observó que la cinética de crecimiento de la descomposición de fase se producía muy lentamente durante las primeras etapas del envejecimiento y aumentaba considerablemente a medida que avanzaba el envejecimiento. Se observó que la ecuación no lineal era más adecuada para describir las primeras etapas de la descomposición espinodal que la lineal.

Aleación Fe-Cr, Descomposición espinodal, Ecuación Cahn-Hilliard, Envejecido térmico

1. Introduction

1.1 Phase Decomposition in the Fe-Cr Alloy System

Figure 1 illustrates the equilibrium diagram for the Fe-Cr alloy system, and it is characterized by an immiscibility gap above which there is a disordered solid solution and below which the solid solution decomposes into Fe-rich clusters and rich in Cr. The dome of the immiscibility gap is between 540 and 630º C. The Fe-Cr system is important in engineering materials, such as in the chemical and nuclear industries, where it is of perpetual interest by becoming brittle when aged at 475 ºC (Weng *et al.* 2003). Zhu *et al.* 1986 were the first to suggest that the spinodal reaction occurs within the immiscibility gap at low temperatures. The morphology of the spinodal decomposition has been difficult to observe in its early stages of transformation, since due to the small elastic deformation between phases and the similarity of the atomic dispersion factors and lattice parameter between Fe and Cr.

Figure 1 Phase diagram of the Fe-Cr system

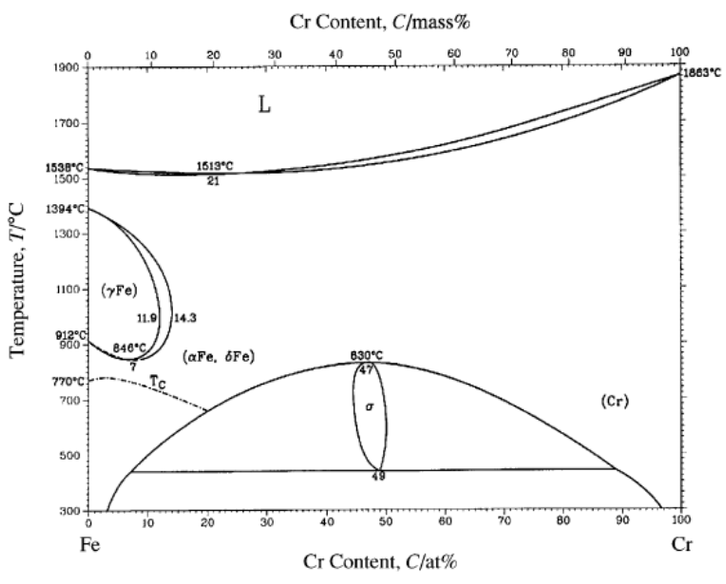

Source (Baker, 2000)

Therefore, the Fe-Cr system is considered as an ideal model system for the study of spinodal decomposition. However, the decomposition kinetics process of these alloys thermodynamically considers other decomposition mechanisms. For example, the decomposition of the alloy (Ustinovshikov *et al.* 2002):

– Fe-20 at 50% at. Cr at 475 ºC is carried out by the spinodal decomposition mechanism, while at 550 ºC by nucleation and growth.
– Fe-24% at. Cr aged at 475ºC proceeds by nucleation and growth.
– Fe-60% at. Cr aged at 475 º C proceeds by spinodal decomposition.

Hyde *et al.* 1995 carried out the analysis of spinodal decomposition in Fe-Cr alloys (see figure 2). The study has three parts: the first details the experimental techniques by ion microscopy, making a three-dimensional reconstruction of the atomic structure of a series of aging treatments at 500°C in Fe-24, 32 and 45% Cr alloys. The second part describes the interconnected microstructure resulting from the spinodal decomposition in a series of aging for the Fe-Cr system whose size and amplitude in composition are analyzed. The third, computer simulation using the Monte Carlo method and a numerical solution based on the Cahn-Hilliard-Cook theory.

Figure 2. Ion microscope micrographs of Fe-Cr alloys aged for 500h at 500°C as a function of Cr content –(a) 19% Cr, (b) 24% Cr, (c) 32% Cr and (d) 45% Cr. The bright regions are enriched in Cr and the dark regions lacking Cr (Miller *et al.* 1995)

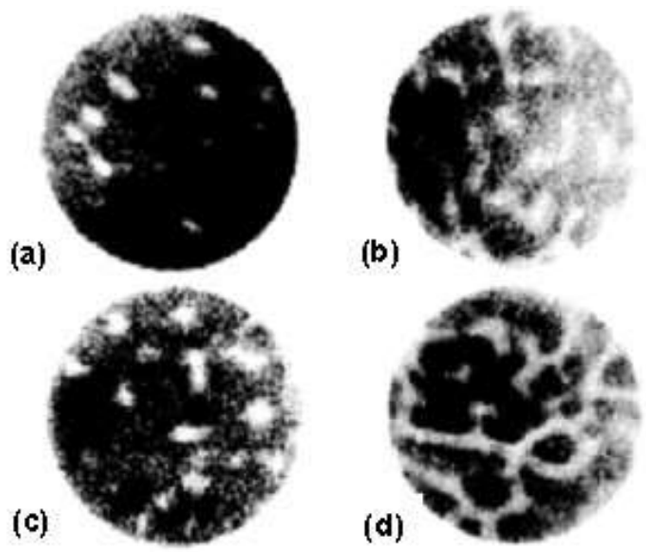

Source (Miller et al. 1995)

Miller *et al.* 1995 studied the phase decomposition at aging temperatures of 400 and 500 °C in Fe-45% Cr alloys. The examined microstructure turned out to be formed by spinodal decomposition. It was found that, at the aging temperature of 500 °C, the activation energy for diffusion was approximately 2.3 eV. However, a similar comparison could not be made for heat treatments of 400 °C, since the transformation kinetics is much slower; but the simulation predicts that the size depends on time, exhibiting a law of behavior with an exponent of time, 0.25.

Ustinovshikov *et al.* 1996 analyzed the formation of phase separation in solid solutions of Fe-Cr alloys. Using transmission electron microscopy and selected area electron diffraction patterns of Fe-(10; 20; 30; 40; 47) wt% Cr alloys treated isothermally at 500 °C (see Figure 3). The solubilized treatments were carried out at a temperature of 1200 °C. They reported some of the structural features, which are not considered for the phase diagram of the Fe-Cr system. These characteristics are the following:

Figure 3 (a) Fe-20%Cr alloy treated at 1200 °C for 1 h and quenched in water. Ion microscopy image showing Cr-rich clusters. (b) Fe-30% Cr alloy thermally treated at 1200°C for 1 h and quenched in water; the sequence of heat treatment at 550°C for 8 h; microstructure separation at low temperature.

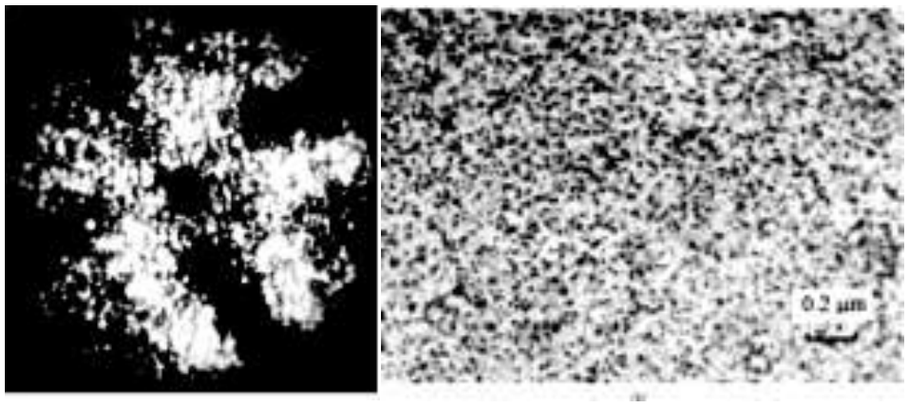

Source (Ustinovshikov et al. 2005)

(A) Many researchers believe that the high-temperature region (1200-1400 ºC) of the Fe-Cr diagram is a region of disordered solid solution. However, thermodynamic studies performed at high temperatures (1040-1400 ºC) showed that the solid solution has a positive deviation from Raoult's law in all study compositions. Therefore, they exhibit a tendency to break down. The different types of microstructures formed under the phase decomposition showed Cr-enriched clusters located in a Cr-depleted matrix. These clusters are of different morphology depending on the thermal treatment and composition. For the 20% Cr and 30% Cr compositions, the embryos have a periodic distribution in the form called “microstructure clusters” oriented along the directions of smooth deformation of the matrix.

(B) When Fe-(30-47) wt% Cr alloys are heat treated in the high temperature region (1200-1400°C) and quenched in water, and subsequently aged in the region of phase formation σ at 600-830º C for different times, the two types of high temperature microstructural separation: $\alpha_1+\alpha_2$ and phase J dissolve completely.

In summary, it can be said that the analysis of spinodal decomposition experimentally has been difficult to perform in the early stages of aging for Fe-Cr alloys. Likewise, the comparison with simulation results has not been an easy task to carry out.

1.2 Phase Field Model

The phase field model was originally developed to study the phenomenon of solidification and other growth processes (Koyama *et al.*, 2006). Unlike the other approaches, the phase field model describes a microstructure by means of a group of field variables from which the spatial distribution of the grains or domains of the different phases and the limits between them can be analyzed. Typical examples of field variables are concentration and the long-range order parameter, which characterize compositional and structural heterogeneities, respectively. To overcome the problems inherent to a moving boundary, the phase field model uses the approximation of a diffuse interface for microstructural evolution (Bhadeshia, 2000).

Three simple examples are presented in Figures 4(a-c) to illustrate the use of field variables that describe different morphologies. In the upper and lower part of the figure, the different morphologies and their corresponding field variable are presented. For example, figure 4(a) to a homogeneous disordered phase with field variable co. Figure 4 (b) shows a mixture of two structurally sized phases described by a non-homogeneous composition field C. Finally, there is a monophase with antiphase domain boundaries characterized by a long-range order parameter η (r). The variables C and η are continuous through the interface between phases or domains.

In the kinetic field model of phases with diffuse interface, the microstructural evolution is described by the spatial and temporal evolution of the field variables moving toward thermodynamic equilibrium, governed by the nonlinear diffusion equation of Cahn and Hilliard and the equation of Allen and Cahn (Cahn *et al.*, 1971, Allen *et al.*, 1979):

$$\frac{\partial c(r,t)}{\partial t} = -M\nabla^2 \left[\frac{\partial F}{\partial c(r,t)} \right] \tag{1}$$

$$\frac{\partial \eta_P(r,t)}{\partial t} = -L_{pq}\nabla^2 \frac{\partial F}{\partial \eta_q(r,t)} \tag{2}$$

Figure 4 Schematic representation of different morphologies and their corresponding field variables

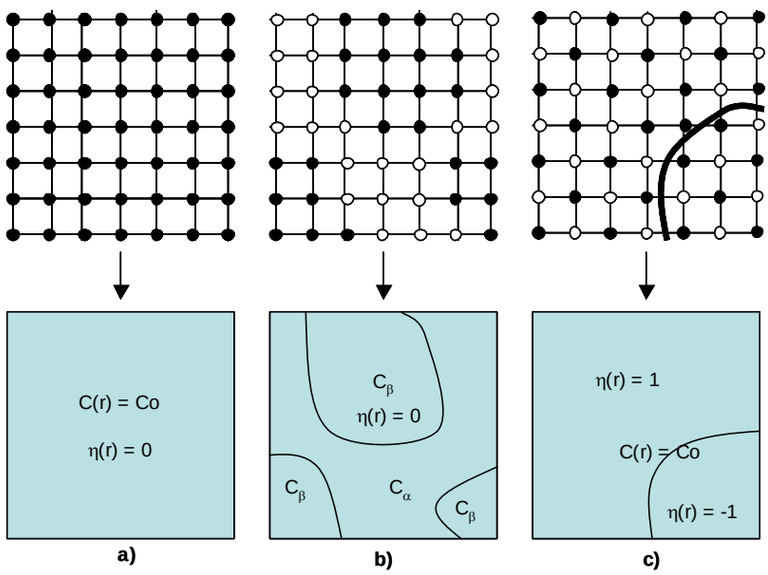

Source (Melo, 2006)

where L_{pq} and M are kinetic coefficients. F is the free energy function in terms of the field variables. The solutions of these equations provide the morphology as well as the kinetic characteristics of the microstructural evolution for a given alloy system. The interfacial boundaries do not need to be specified in advance, but rather emerge with part of the numerical solution. Therefore, the fuzzy interface model offers the flexibility and generality to favorably solve the difficulties faced by the definite interface approach. In the Cahn and Hilliard theory, the interfacial energy is introduced through energy terms due to the compositional gradient. The total free energy F of the inhomogeneous system is given as:

$$F = \int_V \left[f(c) + \frac{1}{2} k\nabla^2 c \right] dV \tag{3}$$

where *f* (c) is the local energy density and k is the gradient energy coefficient, which can be related to the atomic interaction parameters. The derivative of *F* with respect to *C* is as follows:

$$\frac{\partial F}{\partial c} = \frac{\partial f}{\partial c} - k\nabla^2 c \tag{4}$$

Substituting equation (4) into equation (1), the nonlinear Cahn and Hilliard equation is obtained:

$$\frac{\partial c(r,t)}{\partial t} = \nabla \cdot M\nabla \left[\frac{\partial f}{\partial c} - k\nabla^2 c \right] \tag{5}$$

this equation can be solved by finite differences.

Spinodal decomposition in Fe-Cr alloys was studied in Fe-24, 32 and 45% at alloys. Cr, performed by computer simulation by Monte Carlo algorithm methods and by a numerical solution of the Cahn-Hilliard-Cook theory analyzed by Hyde and collaborators (Ustinovshikov *et al.,* 1995). The problem with the Monte Carlo method lies in the ambiguity of time and size measurement. This is a limiting factor in phase decomposition kinetic studies.

Honjo *et al.,* 2000 used a numerical model based on the Cahn and Hilliard linear equation for multicomponent systems that was applied to the prediction of microstructural evolution and phase decomposition in Fe-Cr and Fe-Cr-Mo systems. Figure 5(a) shows the microstructural evolution based on Cr concentration in a Fe-40% at binary alloy. Cr aged at 527°C. The formation of Cr-rich regions by phase decomposition is clearly seen. Their size and interdistance increased with aging time. The Cr concentration profile is shown in Fig. 18(b). The peak amplitudes are equivalent to the Cr equilibrium concentration at 527°C, which was evaluated by Thermo-Calc.

In this study, a numerical simulation model based on the linear, nonlinear, and modified Cahn and Hilliard strain energy equations for the Fe-Cr alloy system at different compositions and temperatures is proposed.

Figure 5 a) Microstructural evolution in a binary alloy Fe-40 % at. Cr aged at 527°C. b) Variation of the Cr concentration profile over time in the Fe-40% at binary alloy. Cr aged at 527°C

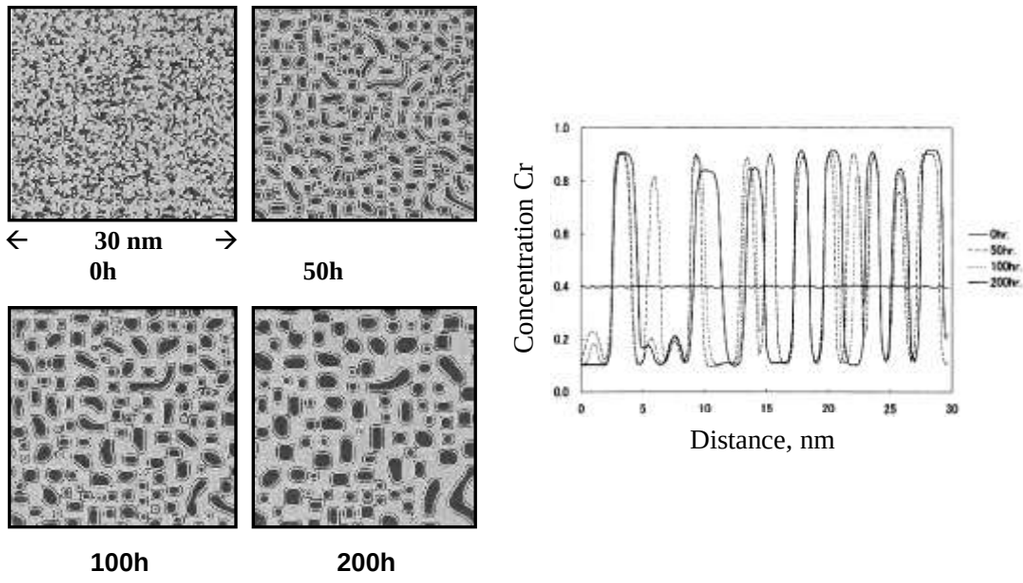

Source (Honjo et al., 2000)

2. Methodology

2.1 Numerical Modeling

In the kinetic field model of phases with diffuse interface, the microstructural evolution is described by the spatial and temporal evolution of the field variables moving towards thermodynamic equilibrium, governed by the Cahn and Hilliard nonlinear diffusion equation in one dimension is the following (Honjo *et al.,* 2000):

$$\frac{\partial c(x,t)}{\partial t} = \nabla \cdot M\nabla\left[\frac{\partial f}{\partial c} - k\nabla^2 c\right] \tag{6}$$

where c is the atomic concentration as a function of position x, *f* is the local free energy, k is the energy coefficient of the compositional gradient, and M is the atomic mobility. This nonlinear equation has been widely used to simulate microstructural evolution in spinodally decomposing alloy systems such as Fe-Cr and Fe-Cr-Mo (Honjo *et al.,* 2000). However, this study does not present the comparison of simulated results with experimental ones.

The Cahn and Hilliard theory for spinodal decomposition is based on the analytical solution of the linear Cahn and Hilliard equation (Cahn *et al.,* 1971):

$$\frac{\partial c(x,t)}{\partial t} = M\left[\left(\frac{\partial^2 f}{\partial c^2} + 2\eta^2 Y\right)\nabla^2 c - 2\kappa\,\nabla^4 c\right] \tag{7}$$

where η is a measure of the mismatch in the lattice parameter a of the decomposed phases and Y is a parameter involving the elastic constants. This linear equation has also been used to follow microstructural evolution and is considered very useful for analyzing the early stages of spinodal decomposition.

For the numerical simulation, the free energy of the Fe-Cr alloy was determined using the model for a regular solution (Honjo *et al.,* 2000):

$$f = f_{Cr}c_{Cr} + f_{Fe}c_{Fe} + \Omega_{Fe-Cr}c_{Cr}c_{Fe} + RT\left[c_{Cr}\ln c_{Cr} + c_{Fe}\ln c_{Fe}\right] \tag{8}$$

where *f*Cr, and *f* Fe, c_{Cr} and c_{Fe} are the free energies in the pure state and the mole fraction of Cr and Fe, respectively. *T* is the temperature and *R* is the gas constant. $\Omega_{Fe\text{-}Cr}$ is the interaction parameter. Table 1 presents the value of the interaction parameter Ω as a function of *T*.

Table 1. Values of the lattice, diffusion, thermodynamic and elastic constants

Constants	Fe-Cr	
Parameter lattice (nm)	a = 0.2866	
Diffusion Coeficient ($cm^2\ s^{-1}$)	D_{Fe} = 1.2 exp (-294000 $Jmol^{-1}$)/RT [63]	
	D_{Cr} = 0.2 exp (-308000 $Jmol^{-1}$)/RT [63]	
$\Omega_{Fe\text{-}Cr}$ (J mol^{-1})	(18600.0+0.1T) [9]	
c_{ij} (J m^{-3}) Fe/Cr	c_{11}=23.10x10^{10} c_{12}=13.54x10^{10} c_{44}=11.78x10^{10}	c_{11}=35.00x10^{10} [64] c_{12}=67.80x10^{10} c_{44}= 10.08x10^{10}
η	0.00614 [63]	

Source: *Own Elaboration*

Atomic mobility M was evaluated according to the following equation (Honjo *et al.,* 2000):

$$\bar{D} = M_i\left(\frac{\partial^2 f_o}{\partial c_i^{\,2}}\right) \tag{9}$$

where the interdiffusion coefficient $\bar{D}$ was defined as (Cahn *et al.,* 1971):

$$\bar{D} = D_{Fe}\,c_{Cr} + (1 - c_{Cr})D_{Cr} \tag{10}$$

The values of the diffusion coefficient D_{Fe} and D_{Cr} are also presented in table 1.

On the other hand, the energy coefficient due to the compositional gradient is defined in the spinodal decomposition theory of Cahn and Hilliard (Cahn *et al.,* 1971) as:

$$K = \left(\frac{2}{3}\right) h_{0.5}^{M}\, r_0^2 \tag{11}$$

where $h_{0.5}^{M}$ is the enthalpy of mixing at c = 0.5 and r_0 is the nearest neighbor distance and is defined as a function of the lattice parameter (a) shown in Table 1.

The elastic strain energy f_{el} was defined, according to the spinodal decomposition theory (Cahn *et al.,* 1971), as follows:

$$f_{el} = A\int \eta^2 Y\left(c - c_0\right)^2 dx \tag{12}$$

where A is the cross-sectional area corresponding to atomic flow, Y is an elastic constant defined by the elastic stiffness constants, c_{11}, c_{12} and c_{44} for the phases rich in Cr and Fe, shown in Table 1. As the difference between the lattice parameters of Fe and Cr is small ($a = (a_{Cr}-a_{Fe})/a_{Fe} = 0.00614$), the elastic strain energy is small and can be approximated to that of an isotropic phase decomposition for which *Y* was defined (Ustinovshikov *et al.*, 1998) as:

$$Y = c_{11} + c_{12} - 2\left(\frac{c_{12}^2}{c_{11}}\right) \tag{13}$$

The elastic constants, c_{ij}, were defined as follows:

$$c_{ij} = c_{ij}^{Cr}\ c_{Cr} + c_{ij}^{Fe}\ \left(1 - c_{Cr}\right) \tag{14}$$

The partial differential equation (14) was solved using the explicit finite difference method (Ustinovshikov *et al.*, 1998) using a computer program in FORTRAN 95 language. A 101 x 101 mesh with a spacing of 0.25 nm was used. The time increment was 10 seconds. The composition of the alloy was Fe-32% at. Cr and that of Fe-40% at. Cr, the aging temperature was 500°C for periods of time in the range of 0 to 1000 h.

Figure 6 shows the diagram of the numerical model of the spinodal decomposition. The data input is the composition of the alloy (conditional on not leaving the miscibility zone characteristic of spinodal decomposition), temperature in Kelvin (K) and time in seconds (s) of the aging treatment. Next, the program calculates the initial solute distribution with the help of a random number generator that allowed obtaining a solute distribution closer to the one that occurs in an alloy in the solubilized and tempered state.

Subsequently, the free energy was calculated based on a regular solution model and with the supplied thermodynamic data. Including the diffusion data, it solves the Cahn and Hilliard linear and nonlinear equation in two dimensions by means of the finite difference method, using a FORTRAN computer program. The data output is the distribution of solute in spatial and temporal form, which allowed obtaining one-dimensional graphs of concentration and precipitation profiles after making two-dimensional graphs of the concentration profiles.

Figure 6 Numerical modeling diagram of the spinodal decomposition

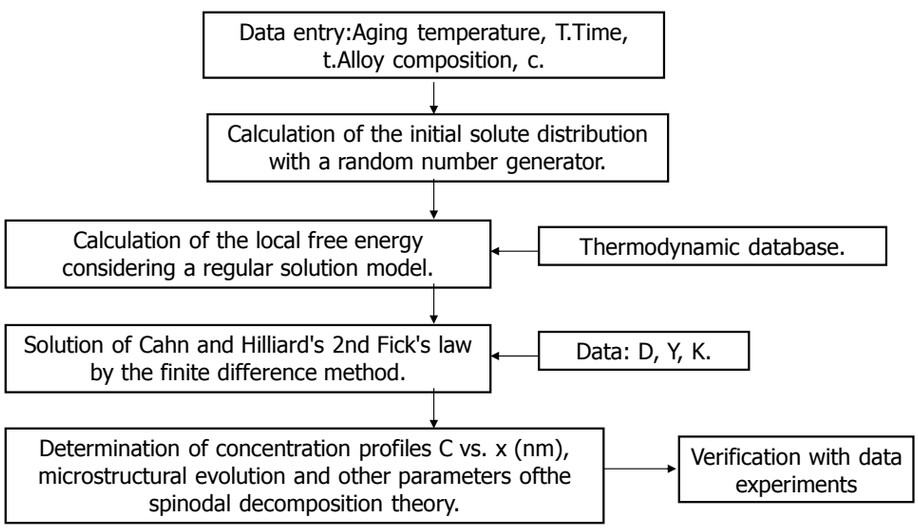

Source: *Own Elaboration*

3. Results

3.1. Simulation with the Cahn and Hilliard Nonlinear Equation

3.1.1 Concentration Profiles

Figures 7 and 8 show the graphs obtained from the simulation using the nonlinear Cahn-Hilliard equation for Cr concentration vs. distance (concentration profiles) for Fe-32% at alloys. Cr and Fe-40% at. Cr at temperatures of 477, 500 and 527°C for different times, respectively.

The profiles for the time of 0 h correspond to the supersaturated solid solution; that is, the alloy in the solution quenched state. A slight fluctuation in the composition for this solubilized condition is observed in the concentration profiles. As the aging time progresses, the increase in the amplitude of the modulation in composition is detected. This behavior clearly indicates that the formation of the phases was carried out by the spinodal decomposition mechanism. Likewise, it can be concluded that the phase decomposition was carried out according to the following reaction:

$$\alpha_{sss} \rightarrow \alpha_1 \text{ (rich Fe)} + \alpha_2 \text{ (rich Cr)} \quad (15)$$

That is, the supersaturated solid solution αsss decomposes spinodally into a mixture of α1 Fe-rich and α2 Cr-rich phases, as predicted by the Fe-Cr equilibrium diagram (Ustinovshikov *et al.*, 1998).

Figure 7 shows the Cr concentration profiles in the Fe-32% at alloy. Cr in this graph is observed for the time of 750 h (figure 7a) a maximum amplitude of the modulation, equilibrium composition. For the concentration profile of the temperature of 500°C (figure 7b) the maximum of the amplitude is observed after 500 h of aging. For the case of the temperature of 527°C (figure 7c), the composition of Fe-32% at. Cr is at the end of the immiscibility gap and is known as an asymmetric alloy. The fluctuation for the solubilized alloy (0 h) decreases with aging time. This suggests that phase decomposition is not taking place, but that there is a homogenization of the composition, since the overall composition of the alloy is outside the spinodal curve for this temperature.

Figure 8 shows the Cr concentration profiles in the Fe-40% at alloy. Cr aged at 477°C, 500° and 527°C for different times. It is observed that there is a maximum amplitude of fluctuation after 750 hours of aging. That is, it approaches the equilibrium composition. For this case, at a temperature of 500°C (figure 8a), the maximum amplitude is observed to occur after 150 h of aging. Likewise, it is observed that the width of the maximum amplitude begins to increase after 500 h. This suggests that the thickening stage of the decomposed phases begins. Figure 8b shows the concentration profiles for the temperature of 527°C, which presents the maximum of the amplitude after 150 h of aging, equilibrium composition. There is still no broadening of amplitude, which indicates that the thickening stage has not yet occurred. It is also presented for the temperature of 500°C.

Figure 7 Cr concentration profiles calculated for the Fe-32%at alloy. Cr aged at 477, 500 and 527ºC for different times

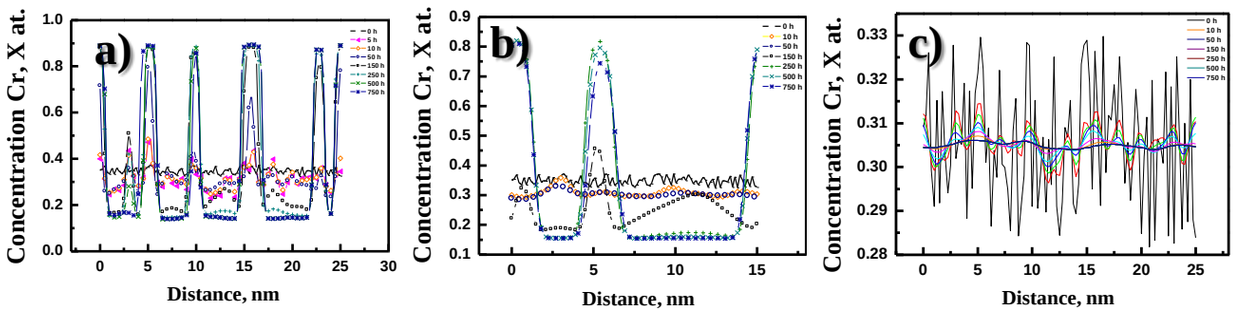

Source: *Own Elaboration*

Figure 8 Cr concentration profiles calculated for the Fe-40% at alloy. Cr aged at 477, 500 and 527ºC for different times

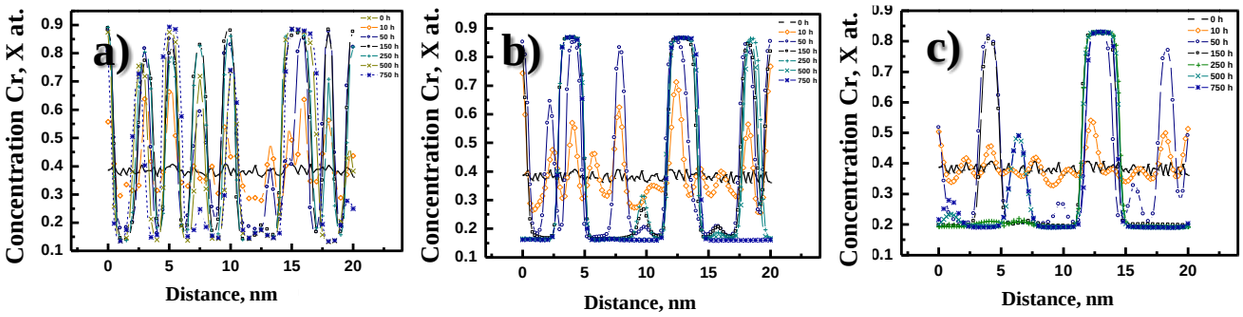

Source: *Own Elaboration*

3.1.2 Microstructural Evolution

Figures 9 to 14 (a-f) show the simulated microstructural evolution, based on Cr concentration, for the Fe-32% at alloys. Cr and Fe-40% at. Cr aged at 477, 500 and 527 ºC, respectively, for different times using the nonlinear equation of Cahn and Hilliard. The dark zones correspond to the phase rich in Cr and the clear ones to the phase rich in Fe. For the Fe-32% at. Cr aged at 477°C for 10 h, figures 9 (a) and (b), it is observed that the phase rich in Cr shows an interconnected morphology (percolation). As the aging continues, it is observed that the volumetric fraction and size of the phase rich in Cr increase and the morphology changes to rounded or ellipsoidal, figures 9 (c) and (f).

Figures 10 (a-f) show the microstructural evolution of the Cr concentration in the Fe-32% at binary alloy. Cr aged at 500ºC for different times. Phase separation in the early stages shows the formation of isolated Cr-enriched islands; Figures 10 (a) and (b). Subsequently, a spheroidal shape is observed, figures 10 (c-f), for the final stages.

Figure 11 shows the microstructural evolution of the Fe-32% at binary alloy. Cr aged at 527ºC for different times. Phase separation for the initial stages shows the formation of isolated islands enriched for Cr concentration; figure 11 (a), later the growth and coalescence of the phase enriched in Cr is observed, in the subsequent times (figure 11 (b-f)). Furthermore, the particles do not exhibit a preferential alignment.

Figure 9 Simulated microstructural evolution for the Fe-32% at binary alloy. Cr aged at 477°C for (a) 10h, (b)50h, (c) 150h, (d) 250h, (e) 500h and (f) 750h

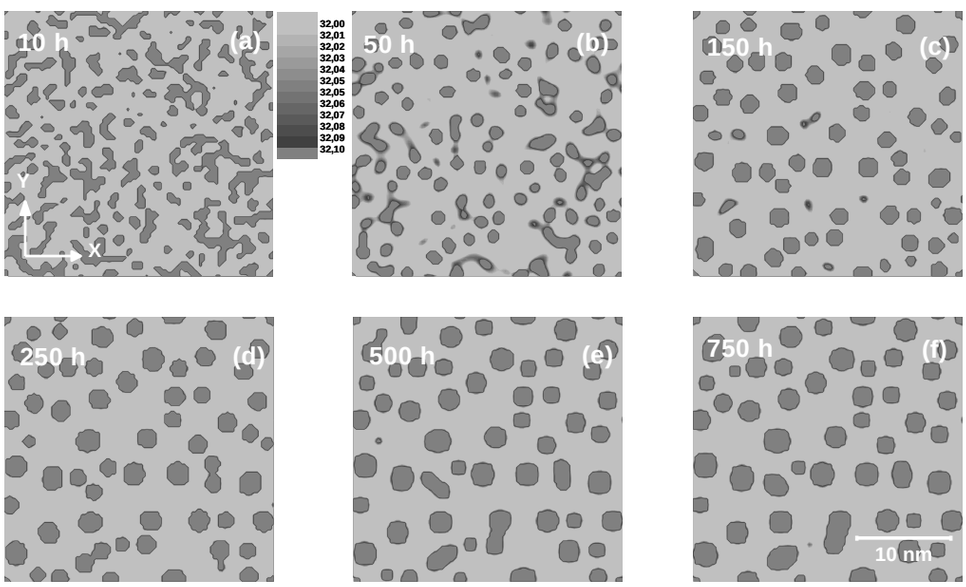

Source: *Own Elaboration*

Figura 10. Evolución microestructural simulada para la aleación Fe-32% at. Cr envejecida a 500ºC por (a) 10 h, (b) 50 h, (c) 150 h., (d) 250 h, (e) 500 h y (f) 750 h

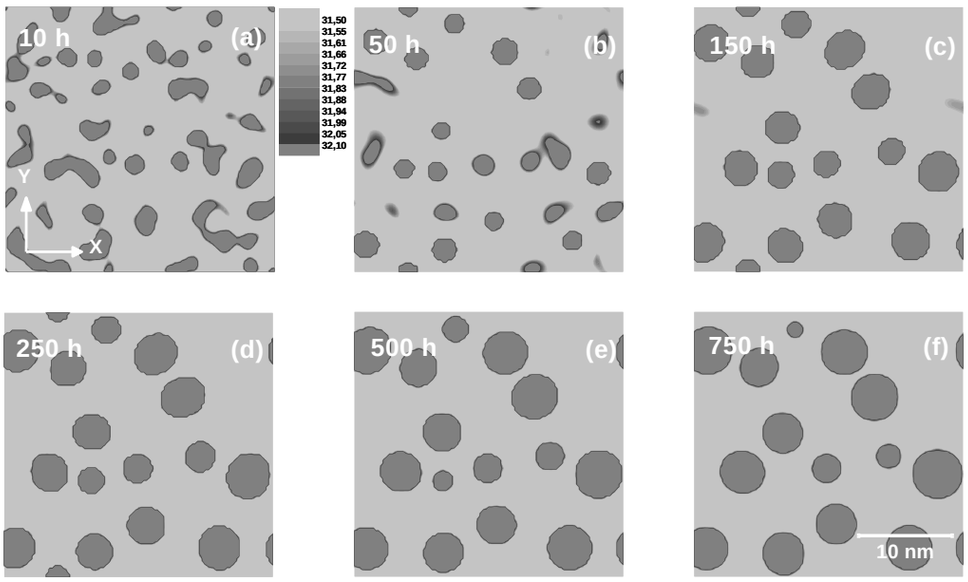

Source: *Own Elaboration*

Figure 11. Simulated microstructural evolution for the Fe-32% at alloy. Cr aged at 527°C for (a) 10h, (b) 50h, (c) 150h, (d) 250h, (e) 500h and (f) 750h

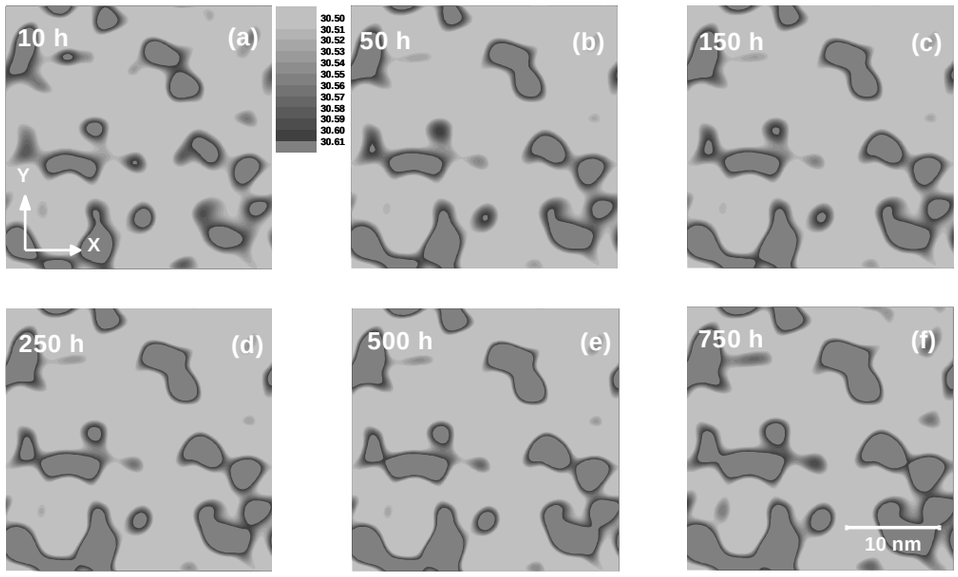

Source: *Own Elaboration*

Figure 12 shows the microstructural evolution for the Fe-40% at alloy. Cr aged at 477°C for different times. In the alloy aged for 10, 50 and 150 h, figures 12 (a-c), it is observed that the morphology of the phase rich in Cr shows an interconnected morphology (percolation). As aging continues, it is observed that the volume fraction and size of the Cr-rich phase increase, and the Cr-rich phase changes morphology to round or ellipsoidal, Figures 12 (d-f).

Figure 13 shows the microstructural evolution of the Cr concentration in the Fe-40% at binary alloy. Cr aged at 500 ºC for different times. The phase separation in the initial stages presents a morphology of isolated islands enriched in Cr concentration, Figure 13 (a) and (b). Subsequently, a change in morphology to rounded or ellipsoid is observed in the final stages. Also, an increase in the volumetric fraction and in the size of the phase rich in Cr is observed.

Figures 14 (a-f) show the microstructural evolution of the Fe-40% at alloy. Cr aged at 527 ºC for different times. The phase decomposition in the initial stage, figure 14 (a), shows an interconnected morphology of the phase enriched in Cr, later to intermediate stages, figure 14 (b-d), the morphology is rounded or ellipsoidal, and in the final stages, Figures 14 (e) and (f)), a spheroidal structure is observed. Also, a decrease in the volumetric fraction is observed, and an increase in the size of the phase rich in Cr.

Figure 12 Simulated microstructural evolution for the Fe-40% at alloy. Cr aged at 477°C for (a) 10h, (b)50h, (c) 150h, (d) 250h, (e) 500h and (f) 750h

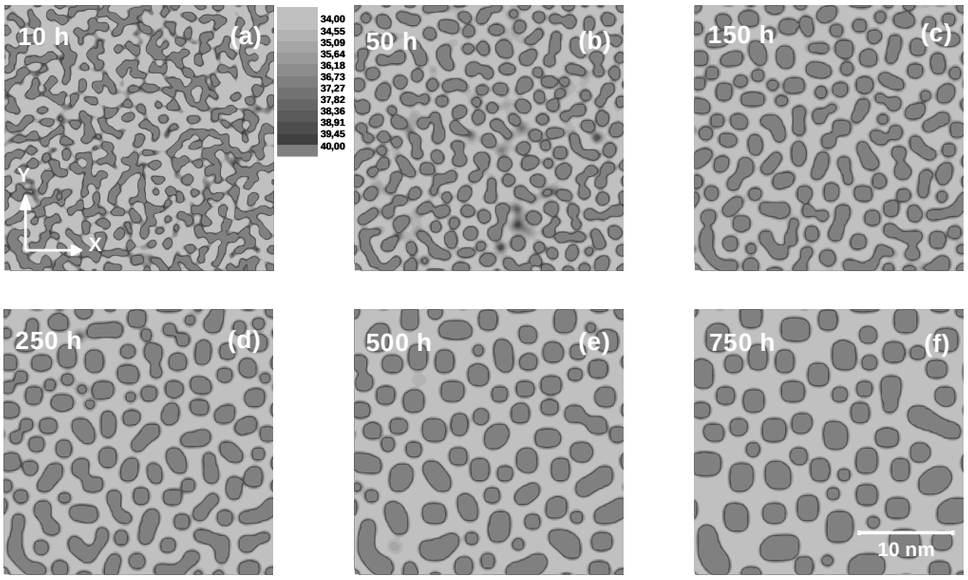

Source: *Own Elaboration*

Figure 13 Simulated microstructural evolution for the Fe-40% at alloy. Cr aged at 500°C for (a) 10h, (b) 50h, (c) 150h, (d) 250h, (e) 500h and (f) 750h

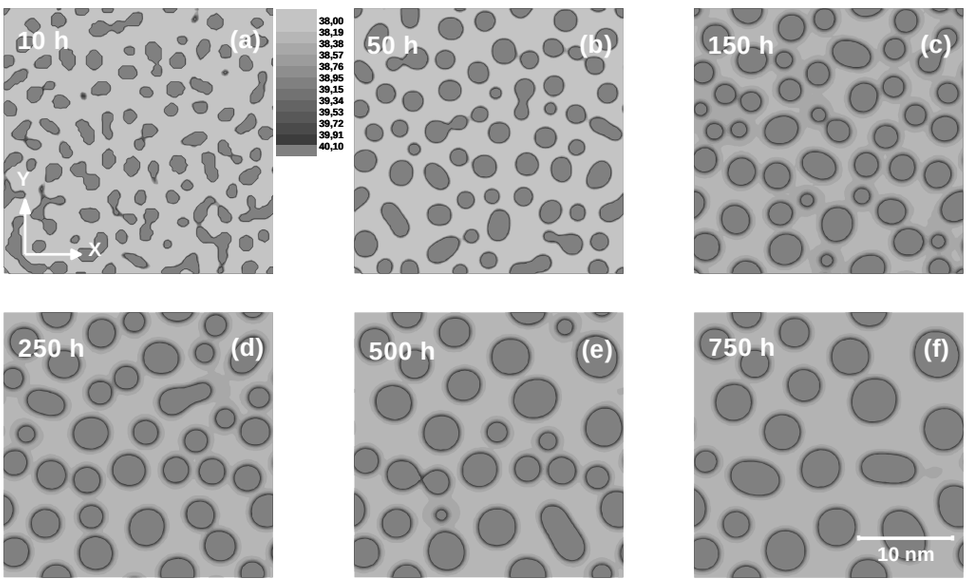

Source: *Own Elaboration*

Figure 14. Simulated microstructural evolution for the Fe-40% at alloy. Cr aged at 527°C for (a) 10h, (b) 50h, (c) 150h, (d) 250h, (e) 500h and (f) 750h.

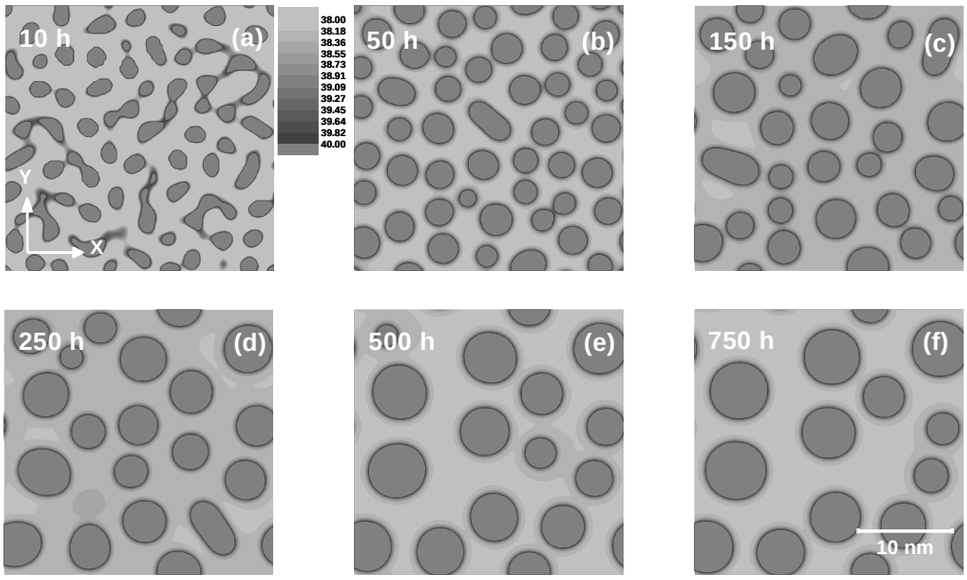

Source: *Own Elaboration*

3.2. Simulation with the Cahn and Hilliard Linear Equation without Considering the Elastic Strain Energy

3.2.1 Concentration Profiles

Figures 15 and 16 show the concentration graphs of Cr vs. distance for Fe-32% at alloys. Cr and Fe-40% at. Cr at temperatures of 477°C, 500°C and 527°C for different times, using the Cahn-Hilliard linear equation without considering the strain energy.

Figures 15 a, b and c show the concentration profiles for the Fe-32% at alloy. Cr aged at 477, 500 and 527 °C, respectively. The profiles present the fluctuations in the composition of the enriched phase of Cr. A maximum in amplitude of concentration is observed in the profiles, which is reached at 150 h at 477°C (figure15a), for 150 h at 500°C (figure 15b) and 50 h at 527°C (figure 15c); balance composition.

From these aging times it is observed that the width of the amplitude begins to increase. So, the thickening stage begins. Also, it is observed for prolonged aging at the three temperatures, the bifurcation phenomenon occurs. That is, the formation of a minimum in the central part of the zone of maximum amplitude of the modulation.

Figure 15 Cr concentration profiles calculated for the Fe-32%at alloy. Cr aged at a) 477°C, b) 500°C and c) 527°C for different times

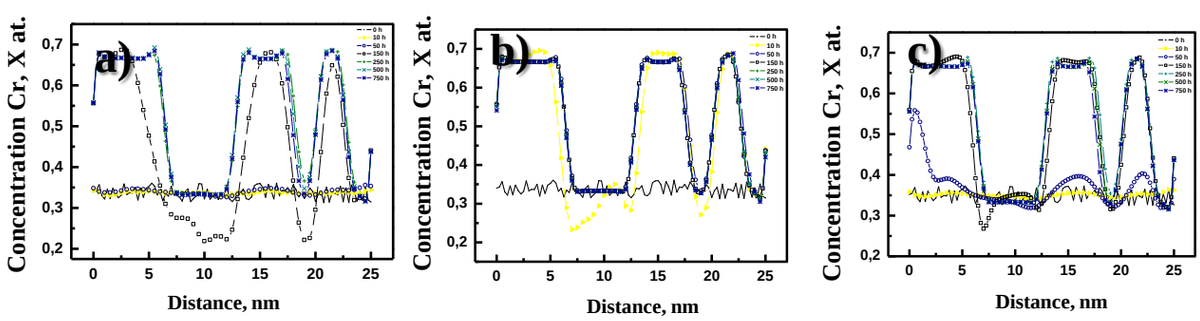

Source: *Own Elaboration*

Figure 16 show the concentration profiles for the Fe-40% at alloy. Cr aged at 477, 500 and 527 °C, respectively. The profiles show the fluctuations in the composition of the Cr-enriched phase. A maximum in the amplitude of the modulation is observed in the profiles, which is reached at 150 h for 477°C (figure 16 a), 150 h for 500°C (figure 16b) and 10 h for 527°C (figure 16c), a composition close to that of equilibrium. From these aging times it is observed that the width of the amplitude begins to increase. This indicates, the beginning of the thickening stage. The profiles figures 16 a, b and c, also present the bifurcation phenomenon at prolonged aging times.

Figure 16 Cr concentration profiles calculated for the Fe-40% at alloy. Cr aged at a) 477°C, b) 500°C, and c) 527°C for different times

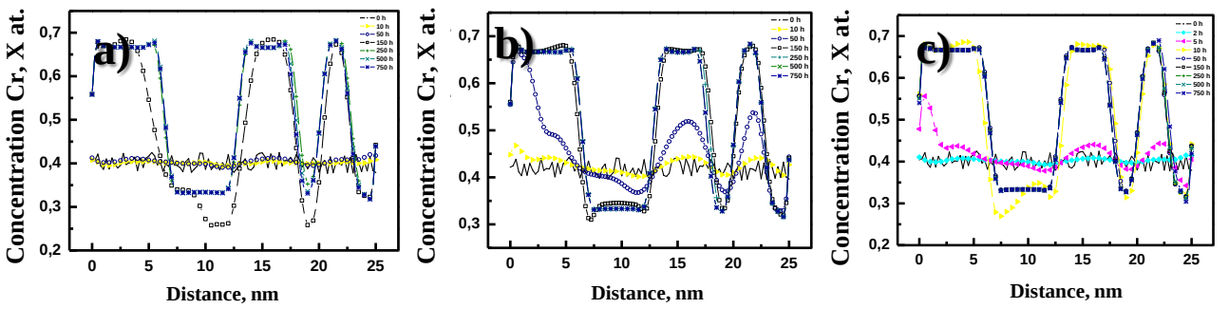

Source: *Own Elaboration*

3.2.2 Microstructural Evolution

Figures 17 to 21 present the simulated microstructural evolution, based on Cr concentration, for Fe-32% at binary alloys. Cr and Fe-40% at. Cr at aging temperatures of 477°C, 500°C and 527°C, respectively, for different times. The dark zones correspond to the phase rich in Cr and the light zone to the phase rich in Fe. Figures 17 (a-f) show the microstructural evolution for the Fe-32% at alloy. Cr aged at 477°C. The morphology presented by the phase rich in Cr at initial times is in the form of isolated islands, figures 17 (a) and (b). Subsequently, the Cr-rich phase changes its morphology to round and elongated plates, which are preferentially aligned in directions parallel to the (x,y) coordinate axes. Also, it is observed that the volumetric fraction and size of the Cr-rich phase increase with aging time, figure 17 (f).

Figures 18 (a-f) show the microstructural evolution of the Cr concentration in the Fe-32% at. Cr aged at 500 ºC for different times. The decomposition of phases in the initial stage, figure 18 (a), presents the formation of the enriched phase of the Cr concentration, which indicates a rounded or ellipsoidal morphology, and an apparent preferential alignment is observed. Subsequently, the intermediate and final stages present the formation of particles with a morphology of elongated plates and preferentially aligned on the directions parallel to the coordinate axes (x, y). Also, it is observed that the volumetric fraction and size of the Cr-rich phase increase with increasing aging time.

Figures 19 (a-f) show the microstructural evolution of the Fe-32% at alloy. Cr aged at 527 ºC for different times. The phase decomposition in the initial stage, figure 19 (a), shows a rounded or ellipsoidal morphology and presents a preferential alignment on the directions parallel to the coordinate axes (x, y). Subsequently, in the intermediate and final stages, the formation of particles with a plate morphology and preferentially aligned is observed. Also, it is observed that the volumetric fraction and size of the phase rich in Cr increase with time.

Figures 20, 21 and 22 present the microstructural evolution of the Fe-40% at alloy. Cr, aged at 477, 500 and 527°C for different times. The morphology observed in the initial stages (figures 20, 21 and 22 (a) and (b), respectively) is like that of the Fe-32% at alloy. Cr for the initial stages. That is, it is rounded and ellipsoidal with an apparent preferential alignment in directions parallel to the (x, y) coordinate axes. Likewise, the morphology that occurs over long periods of time (figures 20, 21 and 22 (c-f), respectively) is rounded and platelike, with an apparent preferential alignment. Also, it is observed that the volumetric fraction, as well as the size of the phase rich in Cr, increase with time.

Figure 17. Simulated microstructural evolution for the Fe-32% at alloy. Cr aged at 477ºC for 10 h, (b) 50 h, (c) 150 h, (d) 250 h, (e) 500 h and (f) 750 h.

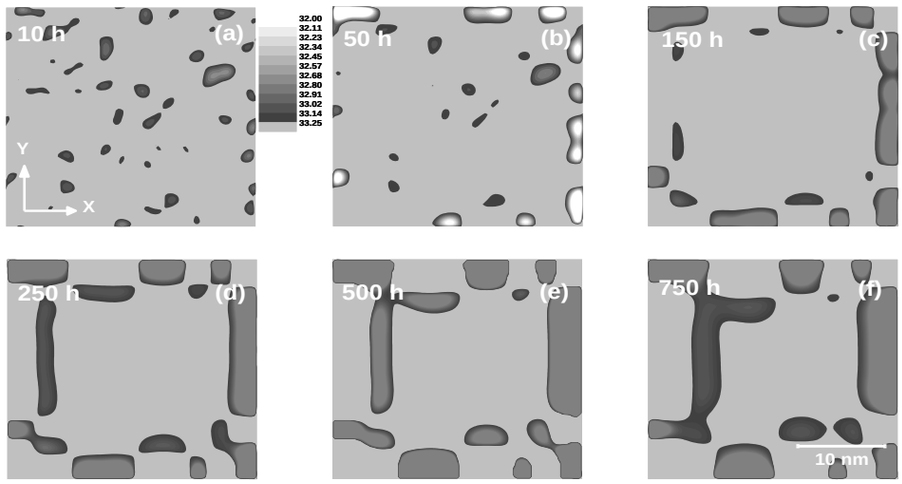

Source: *Own Elaboration*

Figure 18. Simulated microstructural evolution for the Fe-32% at alloy. Cr aged at 500ºC for 10 h, (b) 50 h, (c) 150 h, (d) 250 h, (e) 500 h and (f) 750 h

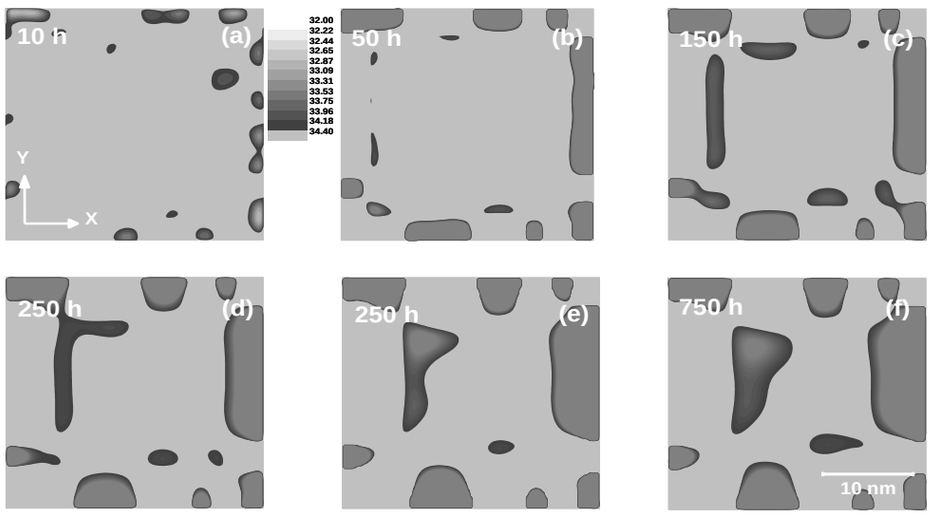

Source: *Own Elaboration*

Figure 19. Simulated microstructural evolution for the Fe-32% at alloy. Cr aged at 527ºC for 10 h, (b) 50 h, (c) 150 h, (d) 250 h, (e) 500 h and (f) 750 h

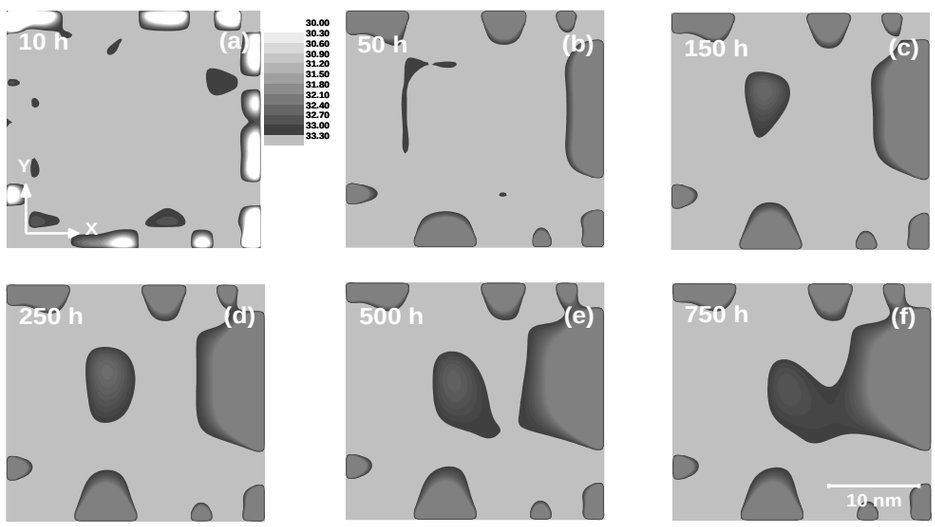

Source: *Own Elaboration*

Figure 20. Simulated microstructural evolution for the Fe-40% at alloy. Cr aged at 477ºC for 10 h, (b) 50 h, (c) 150 h, (d) 250 h, (e) 500 h and (f) 750 h.

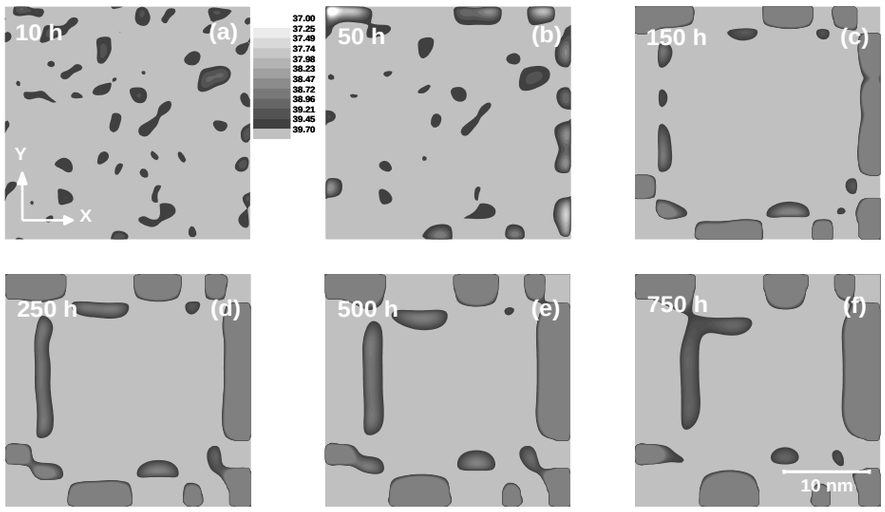

Source: *Own Elaboration*

Figure 21. Simulated microstructural evolution for the Fe-40% at alloy. Cr aged at 500ºC for 10 h, (b) 50 h, (c) 150 h, (d) 250 h, (e) 500 h and (f) 750 h.

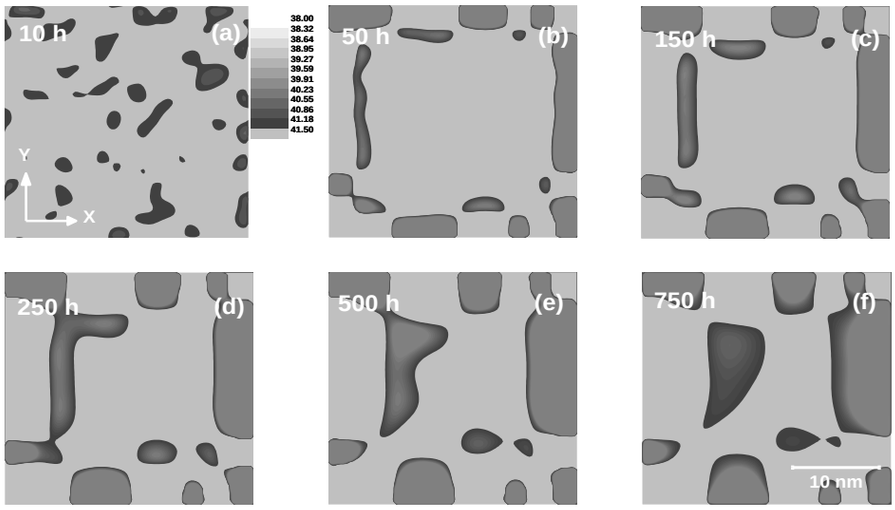

Source: *Own Elaboration*

Figure 22. Simulated microstructural evolution for the Fe-40% at alloy. Cr aged at 527ºC for 10 h, (b) 50 h, (c) 150 h, (d) 250 h, (e) 500 h and (f) 750 h.

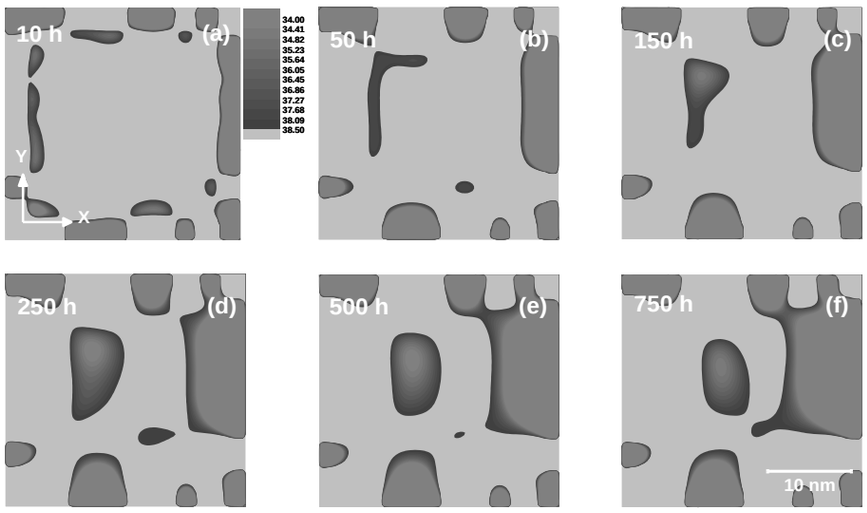

Source: *Own Elaboration*

4. Discussion of Results

4.1. Transformation Mechanisms

The evidence of the fluctuations in composition for the concentration profiles obtained by numerical simulation using the linear equation without considering, and considering the elastic deformation energy, and the non-linear equation of Cahn and Hilliard for the Fe-32% at alloys. Cr and Fe-40% at. Cr aged at 477, 500 and 527 °C for different times, detected the increase in the amplitude of the modulation in composition with the increase in aging time (Meshkov, 2022). This behavior clearly indicates that the formation of the phases was carried out by the spinodal decomposition mechanism (Honjo *et al.*, 2000, Ustinovshikov et al., 2002, Cahn, 1962). Likewise, it can be concluded that the phase decomposition was carried out according to the following reaction:

$\alpha sss \rightarrow \alpha_1$ (rich in Fe) + α_2 (rich in Cr) (16)

That is, the supersaturated solid solution α_{sss} decomposes spinodally into a mixture of α_1 Fe-rich and α_2 Cr-rich phases, as predicted by the Fe-Cr equilibrium diagram (Ustinovshikov et al., 1998).

4.2 Phase Decomposition Kinetics

The results of graph 23 a) and b) of the variation of the wavelength, λ, with the aging time that was obtained for the decomposition kinetics using the linear equation of Cahn and Hilliard considering the energy of elastic deformation. The kinetics of evolution of the modulation in composition indicates that it is faster in the Fe-40% at alloy. Cr than in Fe-32% at. Cr. This is attributed to the fact that the first is located more to the center of the immiscibility gap. It is well known that the driving force for spinodal decomposition is the second derivative of the free energy with respect to composition, d^2G/dx^2 o G´´, and this is more negative for a composition located more in the center of the immiscibility gap, see figure 1. This driving force is what causes the decomposition kinetics to be faster (Hosford, 2005, Cahn, 1968).

Figure 23 also indicates the values of the two slopes that are clearly observed in the decomposition kinetics of Fe-32% at alloys. Cr and Fe-40% at. Cr, see figures 23 a) and 23 b). That is, there is first a slow stage with slopes or time exponent n between 0.13 and 0.19, which is a unique feature in phase decomposition via the spinodal decomposition mechanism. This slow kinetics is attributed to a type of cluster thickening during the early stages and a time growth exponent of 0.16 has been reported (Hirata, 1982), which agrees with the values determined in this study. In contrast, the slope of the kinetics increases to approximately 0.3 for long aging times. According to the thickening theory of Lifshitz, Slyosov, 1961 and Wagner, 1961 (LSW), an exponent of 0.333 is expected for diffusion-controlled thickening (Voorhees, 1992, Cahn, 1992). This suggests that the second stage observed corresponds to the thickening of the decomposed phases. It is important to highlight that this stage is not yet observed for the Fe.32% at alloy. Cr aged at a temperature of 477°C since the decomposition kinetics is slower.

Figure 23 Variation of λ with aging time for alloy a) Fe-32% at. and b) 40%at. Cr aged at 477, 500 and 527°C

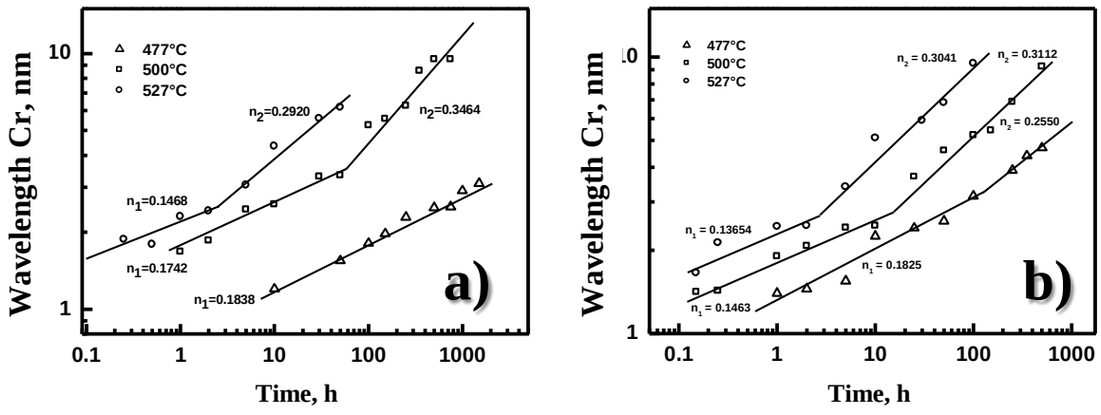

Source: *Own Elaboration*

5. Acknowledgments

We thank the authors to TecNM-TESJo Proyecto 10210.21-PD and participating institutions.

6. Conclusions

Analysis of the spinodal decomposition in Fe-Cr alloys using the nonlinear and linear Cahn-Hilliard equations shows that both equations reproduce the main features of the spinodal decomposition expected in aged Fe-Cr alloys according to the spinodal decomposition theory. However, the morphology of decomposed phases for linear equation simulation is more representative of phase decomposition in the early stages of aging. On the contrary, the nonlinear equation reproduces both the first and the last stages of aging in the aged Fe-Cr alloys.

7. Reference

Baker H. (1992). Alloy Phase Diagrams, ASM Metals Handbook, Vol. 03, 152.

Cahn J. W. (1966). The later stages of spinodal decomposition and the beginnings of particle coarsening, Acta Metallurgica, 14, 1685-1691. https://www.sciencedirect.com/science/article/abs/pii/0001616066900216?via%3Dihub, https://doi.org/10.1016/0001-6160(66)90021-6

Cahn J.W. and Hilliard J.E. (1971). Spinodal decomposition: A reprise, Acta Metallurgica, 19(2), 151-161. https://www.sciencedirect.com/science/article/abs/pii/0001616071901271?via%3Dihub, https://doi.org/10.1016/0001-6160(71)90127-1

Cahn J. W. (1962). On spinodal decomposition in cubic crystals, Acta Metallurgica, Vol.10, 179-183. https://www.sciencedirect.com/science/article/abs/pii/0001616062901141?via%3Dihub, https://doi.org/10.1016/0001-6160(62)90114-1

Cahn J. W. (1968). Spinodal Decomposition, Transactions of the Metallurgical Society of AIME, Vol. 242, 166-180. https://onlinelibrary.wiley.com/doi/abs/10.1002/9781118788295.ch10

Hirata V. M. L. (1982) Ph.D. Thesis, Tohoku University, Japan.

Hyde J. M., Hetherington M. G., Cerezo A. and Smith G. D. W. and Elliott C. M. y Miller M. K. (1995). Spinodal decomposition in Fe-Cr alloys: experimental study at the atomic level and comparison with computer models--I. Introduction and methodology, Acta Metallurgica et Materialia, 43(9), 3385-3401. https://www.sciencedirect.com/science/article/abs/pii/0956715195000403?via%3Dihub, https://doi.org/10.1016/0956-7151(95)00040-3

Honjo M. and Saito Y., Numerical simulation of phase separation in Fe-Cr binary and Fe-Cr-Mo ternary alloys with use of the Cahn-Hilliard equation, ISIJ Internacional, Vol. 40, No.9, 2000, 914-919. https://www.jstage.jst.go.jp/article/isijinternational1989/40/9/40_9_914/_article, DOI:10.2355/ISIJINTERNATIONAL.40.914

Hosford. W. F. (2005) Physical Metallurgy, Taylor & Francis, EE.UU, 49-69. https://www.taylorfrancis.com/books/mono/10.1201/b15858/physical-metallurgy-william-hosford, https://doi.org/10.1201/b15858

Koyama T. and Onodera H. (2006). Modeling of microstructure changes in Fe−Cr−Co magnetic alloy using the phase-field method, Journal of Phase Equilibrium and Diffusion, 27(1) 22-29. https://link.springer.com/article/10.1361/105497106X92763, DOI: 10.1361/105497106X92763

Lifshitz I. M. and Slyosov V.V. (1961). The kinetics of precipitation from supersaturated solid solutions", J. Phys. Chem. Solids. 19, 35-50. https://www.sciencedirect.com/science/article/abs/pii/0022369761900543?via%3Dihub, https://doi.org/10.1016/0022-3697(61)90054-3

Meshkov E.A., and Yanilkin A.V., New method of atomistic modeling of α−α′ phase transition in Fe–Cr alloy with effective accounting for vibrational entropy, Computational Materials Science.Vol. 212, 2022. https://www.sciencedirect.com/science/article/abs/pii/S0927025622003111?via%3Dihub,https://doi.org/10.1016/j.commatsci.2022.111563

Miller M. K., Hyde J. Cerezo M., A. and Smith G. D. W., Comparison of low temperature decomposition in Fe-Cr and duplex stainless steels, Applied Surface Science, Vol. 87-88, 1995, 323-328. https://doi.org/10.1016/0169-4332(95)00497-1

Qin R. S. and Bhadeshia H. K. (2010) Phase Field Modelling. Materials Science and Technology, 26(7), 803-813. https://www.tandfonline.com/doi/abs/10.1179/174328409X453190, DOI 10.1179/174328409X453190

Ustinovshikov Y. and Pushkarev B. (2005). Alloys of the Fe–Cr system: the relations between phase transitions "order–disorder" and "ordering-separation", Journal of Alloys and Compounds, 389, 1-2, 95-101. https://www.sciencedirect.com/science/article/abs/pii/S0925838804010370?via%3Dihub, https://doi.org/10.1016/j.jallcom.2004.07.050

Ustinovshikov Y., Pushkarev B. and Sapegina I. (2005). Conditions of existence of a disordered solid solution having chemical interactions between the atomic species Fe-Cr, Journal of Alloys and Compounds, 394 (1-2), 200-206. https://www.sciencedirect.com/science/article/abs/pii/S0925838804014008?via%3Dihub, https://doi.org/10.1016/j.jallcom.2004.10.033

Ustinovshikov Y. and Pushkarev B. (1998). Morphology of Fe–Cr alloys, Materials Science and Engineering A, 241 (1-2), 159-168. https://www.sciencedirect.com/science/article/abs/pii/S092150939700484X?via%3Dihub, https://doi.org/10.1016/S0921-5093(97)00484-X

Ustinovshikov Y., B Pushkarev. and Igumnov I., Fe-rich portion of the Fe-Cr phase diagram: electron microscopy study, Journal of Materials Science, Vol. 37, 2002, 2031-2042. https://link.springer.com/article/10.1023/A:1015259517812, https://doi.org/10.1023/A:1015259517812

Y. Ustinovshikov, M. Shirobokova and B. Pushkarev, A structural study of the Fe-Cr system alloys, Acta Materiallia, Vol. 44, No. 12, 1996, 5021-5032. https://www.sciencedirect.com/science/article/abs/pii/S1359645496000882?via%3Dihub, https://doi.org/10.1016/S1359-6454(96)00088-2

Voorhees P. W., Ostwald ripening of two-phase mixtures, Annu. Rev. Mater. Sci., Vol. 22, 1992, 197-215. https://www.annualreviews.org/doi/10.1146/annurev.ms.22.080192.001213, https://doi.org/10.1146/annurev.ms.22.080192.001213

Wagner V. C. (1961). Theorie der Alterung von Niederschlägen durch Umlösen. Z Elektrochemic, 65, 581-591. https://onlinelibrary.wiley.com/doi/10.1002/bbpc.19610650704, https://doi.org/10.1002/bbpc.19610650704

Weng, Chen and Yang (2003). The high-temperature and low-temperature aging embrittlement in a 2205 duplex stainless steel, Bulletin of the College of Engineering, N.T.U., No. 89, 45-61. https://www.nrc.gov/docs/ML1004/ML100491406.pdf

Zhu F., Haasen P. and Wagner R., An atom probe study of the decomposition of Fe-Cr-Co permanent magnet alloys, Acta Metallugica. Vol. 34, 1986, 457-463. https://www.sciencedirect.com/science/article/abs/pii/0001616086900817?via%3Dihub, https://doi.org/10.1016/0001-6160(86)90081-7